

LASER INTERFEROMETER GRAVITATIONAL WAVE OBSERVATORY  
- LIGO -

CALIFORNIA INSTITUTE OF TECHNOLOGY  
MASSACHUSETTS INSTITUTE OF TECHNOLOGY

<b>Document Type</b> <b>LIGO-T980029-01 - D</b> 5/12/98
<b>Effect of Beamsplitter Vibration Resonance Excitation on the Optically Sensed Cavity Length</b>
D. Coyne

*Distribution of this draft:*

Detector

This is an internal working note  
of the LIGO Project.

**California Institute of Technology**  
**LIGO Project - MS 51-33**  
**Pasadena CA 91125**  
Phone (818) 395-2129  
Fax (818) 304-9834  
E-mail: info@ligo.caltech.edu

**Massachusetts Institute of Technology**  
**LIGO Project - MS 20B-145**  
**Cambridge, MA 01239**  
Phone (617) 253-4824  
Fax (617) 253-7014  
E-mail: info@ligo.mit.edu

WWW: <http://www.ligo.caltech.edu/>

## Abstract

Any (unintended) magnetic coil drive currents at the beamsplitter resonances will be amplified by the high Q of the beamsplitter. The transfer function of applied force at the magnet positions to TEM<sub>00</sub> displacement response of the front surface of the LIGO beamsplitter is calculated (based upon finite element structural dynamics computation). The gain attenuation required in the length control system, in order to prevent driving the beamsplitter motion at resonance beyond acceptable limits, may be established from the transfer function.

*Keywords:* beamsplitter, eigenvectors, mode shapes, frequencies, length control, LSC

**Revision 01:** Added an explanation of the possible refractive offset displacement value and an explanation for the higher values of the Gaussian-weighted integral when the beam is centered as opposed to offset from the center. Also made the coordinate axes in Figure 1 readable. Removed an incorrect comment (at the end of section 5) regarding reduction by the cavity finesse.

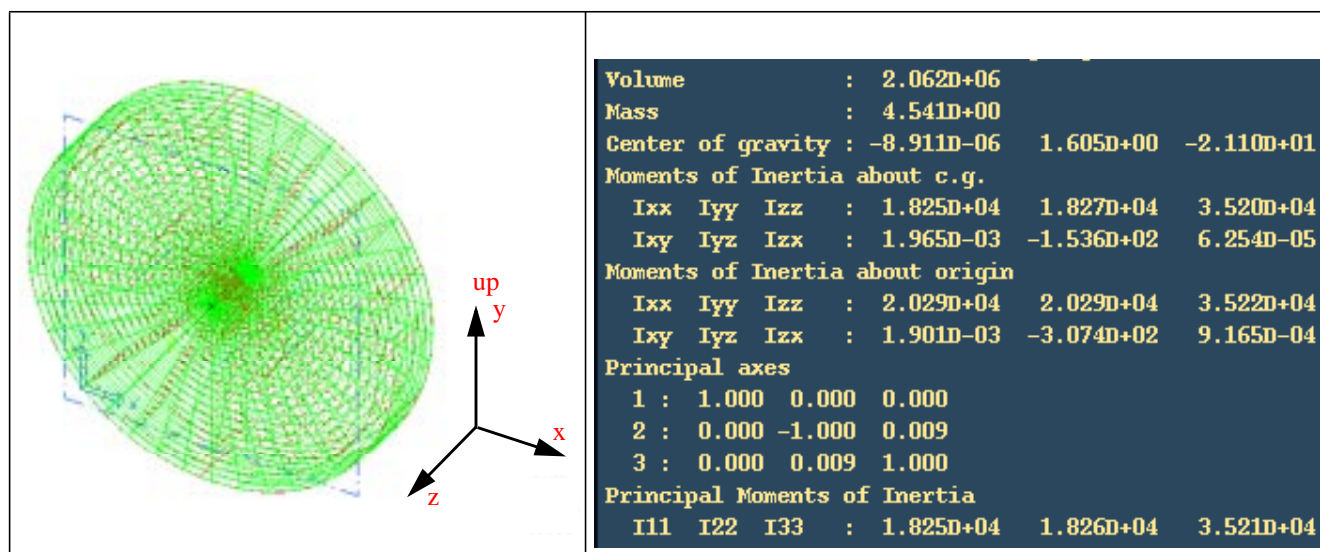
## 1 INTRODUCTION

The analytical derivation of the effect upon the TEM<sub>00</sub> cavity mode due to driving the beamsplitter at one or more of its resonance frequencies has been described in a previous technical memorandum<sup>1</sup> on the End Test Mass (ETM). This same methodology is applied here to the beamsplitter (BS) which has lower resonant frequencies.

## 2 BEAMSPLITTER FINITE ELEMENT MODEL

The Beamsplitter (BS) finite element model is indicated in Figure 1. The optic is a 250 mm diameter, 40 mm thick (at its minimum) fused silica cylinder with one face wedged at a 1 degree angle<sup>2</sup>. The 50/50 beam splitting coating is on the front face and the magnet/standoff assemblies (used for voice coil actuation and control) are on the back face. The model is composed of 6240 linear solid brick elements and has the mass properties shown in Figure 1.

Figure (1) Finite Element Model, Coordinate System and Mass Properties (units are mm and kg)



1. D. Coyne, "Test Mass Transmissibility", LIGO-T970191-03, 2/10/98.

2. LIGO Drawing D960789-B, Beam Splitter Substrate.

The four magnet positions are at a radial distance of 114.3 mm and at 45, 135, 225 and 315 degrees from the +X (horizontal) axis. The dynamic model does not include the beveled edge of the optic, nor does it include the four dumbbell magnet standoff and magnet assemblies. The boundary condition for the eigenvalue analysis is free (unconstrained); The first six modes are zero frequency, rigid body modes.

The material property data used for the fused silica is indicated in Table 2.

**Table 1. Fused Silica Property Data**

<i>Property</i>	<i>Units</i>	<i>Value</i>
Elastic Extensional Modulus, E	mN/mm <sup>2</sup>	7.3 x 10 <sup>7</sup>
Elastic Shear Modulus, $G = \frac{E}{2(1 + \nu)}$	mN/mm <sup>2</sup>	3.1 x 10 <sup>7</sup>
Poison's ratio, $\nu$	-	0.17
Density, $\rho$	Kg/mm <sup>3</sup>	2.202 x 10 <sup>-6</sup>
Quality factor <sup>a</sup> , Q	-	1.3 x 10 <sup>6</sup>

a. S. Kawamura, et. al., LIGO-T970158-06-D

### 3 NATURAL MODES

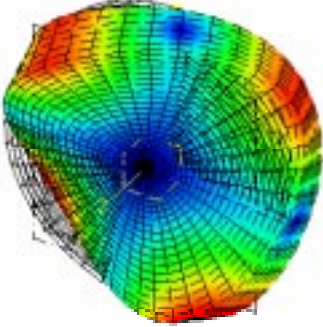
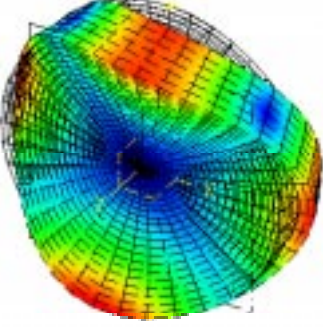
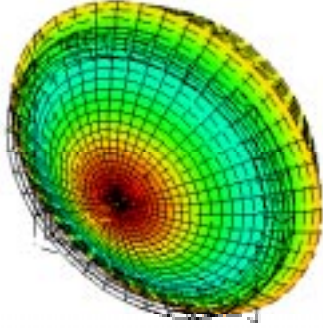
The natural modes shapes, frequencies, modal mass and modal stiffness are indicated in Table 1. The analysis indicates a non-axisymmetric pair of modes with astigmatic shape at 3.78 kHz, the first symmetric (drum head) mode at 5.58 kHz, then 5 pairs of non-axisymmetric modes before the second symmetric (radial contraction) mode at 14.6 kHz. By comparison, the ETM has two astigmatic modes at 6.6 kHz, a drum head mode at 9.2 kHz, then 4 pairs of non-axisymmetric modes before the radial contraction mode at 14.5 kHz. Since the BS is thinner than the ETM, its bending stiffness is reduced and the lower BS frequency of the drum head mode and the additional non-axisymmetric mode pair between the 1st and 2nd symmetric modes is expected.

The eigenvalue analysis results presented herein are the result of a “consistent” mass matrix formulation, rather than a “lumped” mass matrix.<sup>1</sup> Previous analysis (Ref. [1]), on the Input Test Mass (ITM) was based upon a lumped mass matrix. For the BS, the frequencies calculated with a consistent mass matrix (i.e. the more realistic case) are from 1% to 6% higher than the lumped mass case; This may explain the ~1% lower first frequency by analysis compared to measurement reported in Ref. [1] for the ETM.

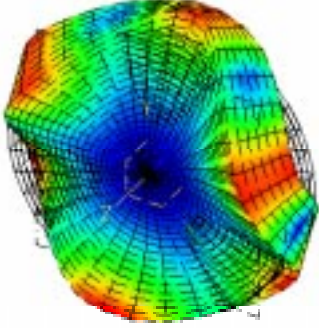
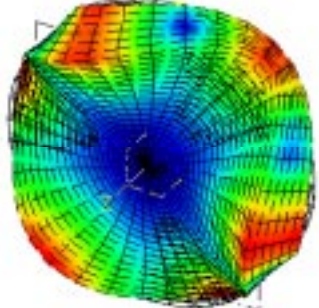
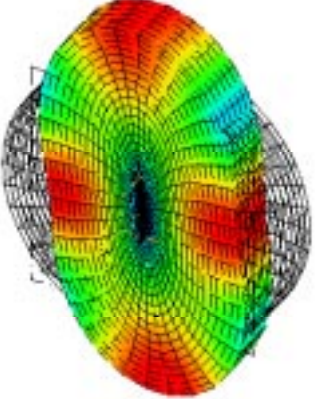
---

1. See for example, K. Bathe, Finite Element Procedures in Engineering Analysis, Prentice-Hall, 1982, pp. 162-163, for an explanation of consistent and lumped mass matrices.

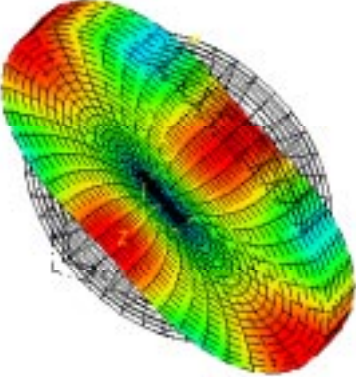
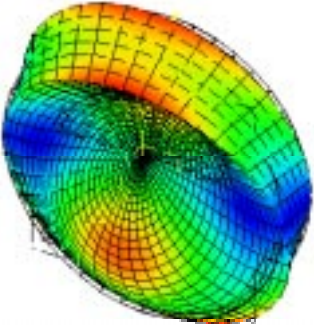
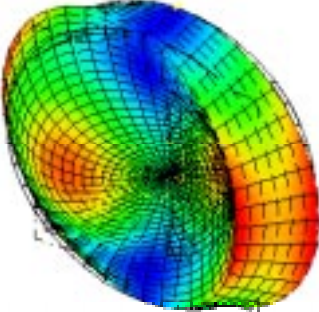
**Table 2. BS Calculated Modes**

#	<i>Mode Shape</i>	<i>Frequency (Hz)</i>	<i>Modal Mass (<math>10^6</math> gm)</i>	<i>Modal Stiffness (<math>10^{15}</math> N/m)</i>
7		3785	0.865	0.489
8		3785	0.851	0.481
9		5578	1.25	1.54

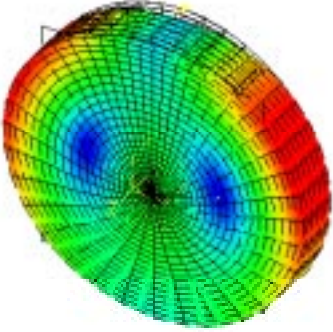
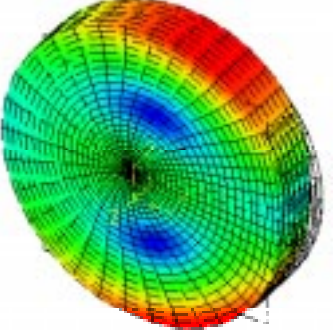
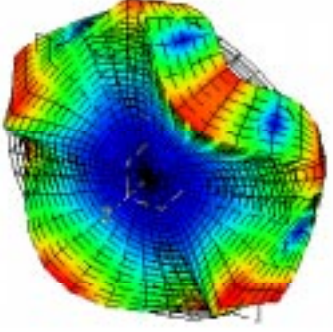
**Table 2. BS Calculated Modes**

#	<i>Mode Shape</i>	<i>Frequency (Hz)</i>	<i>Modal Mass (<math>10^6</math> gm)</i>	<i>Modal Stiffness (<math>10^{15}</math> N/m)</i>
10		7975	0.735	1.85
11		7975	0.756	1.90
12		11259	2.17	10.9

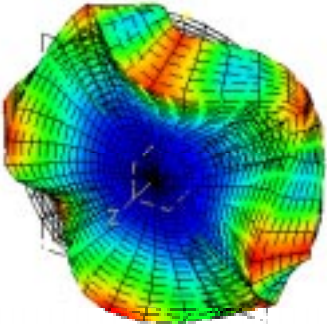
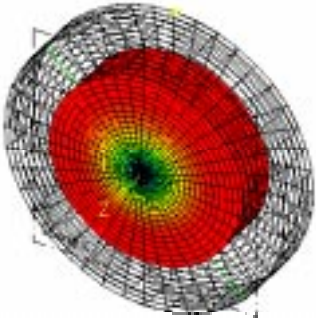
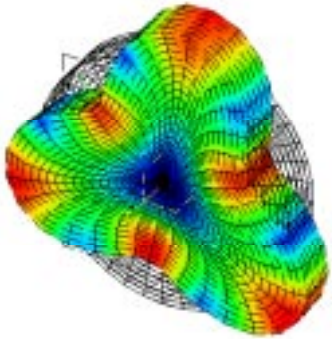
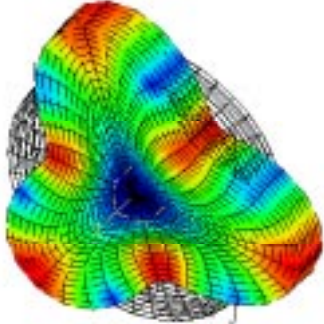
**Table 2. BS Calculated Modes**

#	<i>Mode Shape</i>	<i>Frequency (Hz)</i>	<i>Modal Mass (<math>10^6</math> gm)</i>	<i>Modal Stiffness (<math>10^{15}</math> N/m)</i>
13		11259	3.26	16.3
14		11332	1.08	5.47
15		11334	1.13	5.73

**Table 2. BS Calculated Modes**

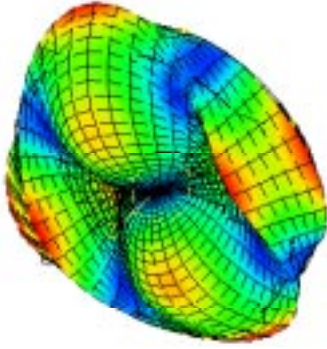
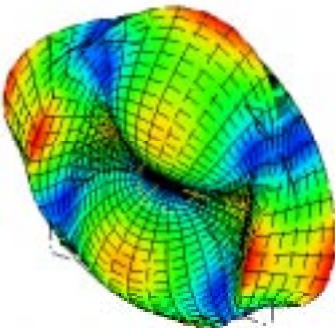
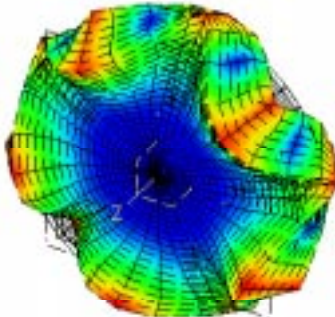
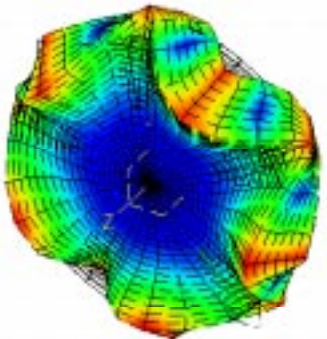
#	<i>Mode Shape</i>	<i>Frequency (Hz)</i>	<i>Modal Mass (<math>10^6</math> gm)</i>	<i>Modal Stiffness (<math>10^{15}</math> N/m)</i>
16		12674	1.16	7.34
17		12677	1.11	7.07
18		12760	0.702	4.51

**Table 2. BS Calculated Modes**

#	Mode Shape	Frequency (Hz)	Modal Mass ( $10^6$ gm)	Modal Stiffness ( $10^{15}$ N/m)
19		12760	0.651	4.18
20		14629	3.20	27.1
21		17283	1.46	17.2
22		17283	1.56	18.3



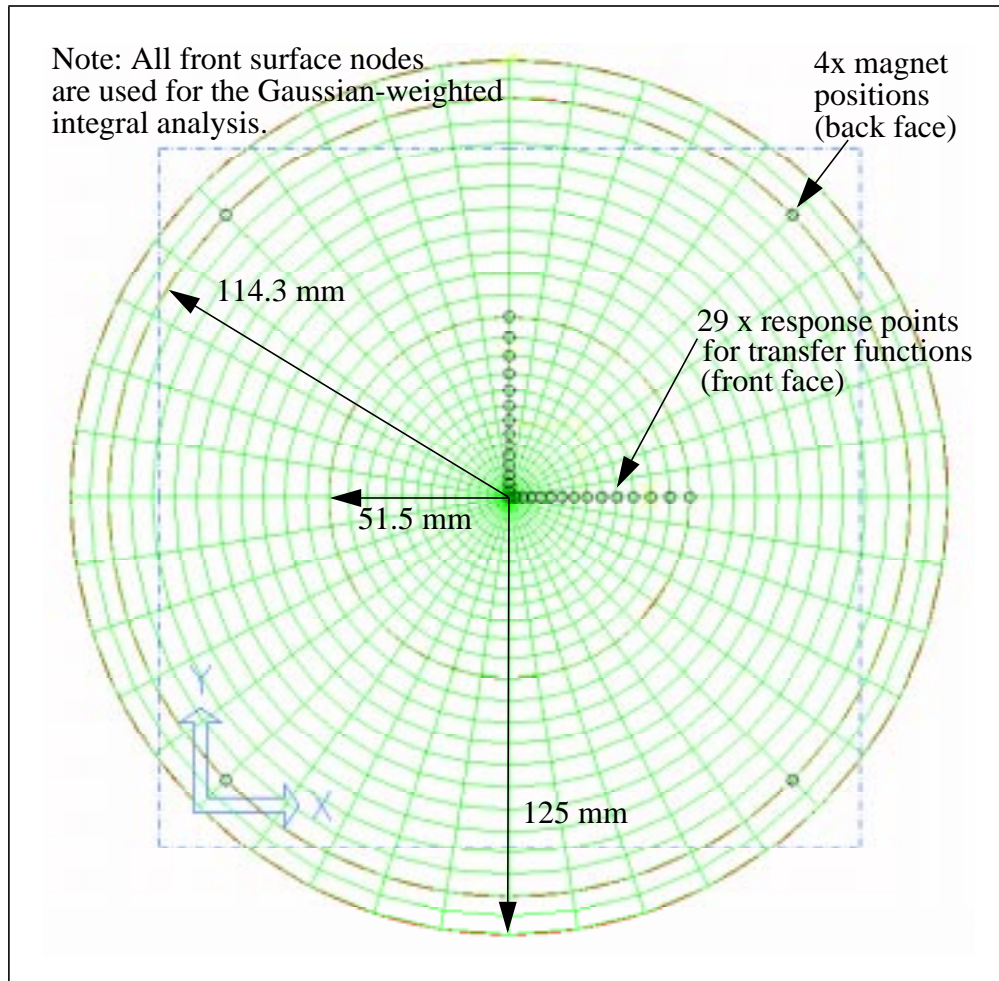
**Table 2. BS Calculated Modes**

#	Mode Shape	Frequency (Hz)	Modal Mass ( $10^6$ gm)	Modal Stiffness ( $10^{15}$ N/m)
23		17388	1.15	13.7
24		17388	1.15	13.8
25		17958	0.575	7.32
26		17958	0.576	7.33

## 4 TRANSFER FUNCTION

In the frequency response analysis, the magnet/voice coil force is assumed to act in the direction parallel to the beamsplitter cylindrical axis despite the fact that the magnet's axis is normal to the wedged surface. The steady-state transfer function (ratio of response displacement to driving force) is given for coherently forcing at the four magnet positions (on the backface of the beamsplitter) with response at the 21 points (on the front face of the beamsplitter) indicated in Figure 2.

Figure (2) Response & Excitation Points



The resulting transfer functions (surface point displacements for magnet point forces) are indicated in Figure 3, as calculated by the IDEAS dynamic response module. The amplitude of response at resonance is not calculated well in these transfer functions for high-Q systems such as the beamsplitter. The frequency sampling,  $\Delta\omega$ , required to capture the amplitude at resonance,  $\omega_0$ , is approximately:

$$\frac{\Delta\omega}{\omega_0} \approx \frac{1}{Q} \quad (1)$$

For a  $Q=1 \times 10^6$ , and a resonance of  $f_0 = 5$  kHz, this implies  $\Delta f \sim 5$  mHz or 3 million samples over a 15 kHz range, which is a prohibitively long calculation.

The frequency response can be computed through the summation of modal responses:

$$\{\gamma\} = \sum_{k=1}^n \frac{\{F_k\}}{m_k(\omega_k^2 + 2i\zeta\omega\omega_k - \omega^2)} \quad (2)$$

where,

$m_k$  = modal mass

$\gamma$  = modal displacement

$\zeta$  = effective modal viscous damping ratio

$\omega_k$  = natural frequency

$F_k$  = modal (generalized) force

$\omega$  = frequency

subscript  $k = k^{\text{th}}$  mode

At a resonance frequency,  $\omega_0$ :

$$\{\gamma(\omega_0)\} = \sum_{k=1}^n \frac{\{F_k\}}{m_k(\omega_k^2 + 2i\zeta\omega_0\omega_k - \omega_0^2)} \quad (3)$$

or, approximately,

$$\gamma_0 = \frac{F_0}{2im_0\omega_0^2\zeta} \quad (4)$$

The generalized forces (for unrestrained boundary conditions) are:

$$\{F_k\} = [\varphi]^T \{F_e\} \quad (5)$$

where,

$[\varphi]^T$  = mode displacement matrix (mode shapes)

$\{F_e\}$  = applied forces (excitation)

Similarly, the physical displacement is given by:

$$\{\delta\} = [\varphi]^T \{\gamma\} \quad (6)$$

or, the displacement at a response point,  $r$ , at resonance,  $\omega_0$ , is given as follows:

$$\delta_{r0} = \Phi_{r0}\gamma_0 = \Phi_{r0}\left(\frac{F_0}{2im_0\zeta\omega_0^2}\right) = \Phi_{r0}\left(\frac{\{\Phi_0\}^T\{F_e\}}{2im_0\zeta\omega_0^2}\right) \quad (7)$$

$$|\delta_{r0}| = \Phi_{r0}\left(\frac{\{\Phi_0\}^T\{F_e\}}{2m_0\zeta\omega_0^2}\right) \quad (8)$$

If we denote the modal coefficients at each of the 4 magnet positions at the resonance,  $\omega_k$ , as  $\{\Phi_{ke1}, \Phi_{ke2}, \Phi_{ke3}, \Phi_{ke4}\}$  then the transfer function at a response position,  $\delta_r$ , for a unit force (at each of the 4 magnet positions) is as follows:

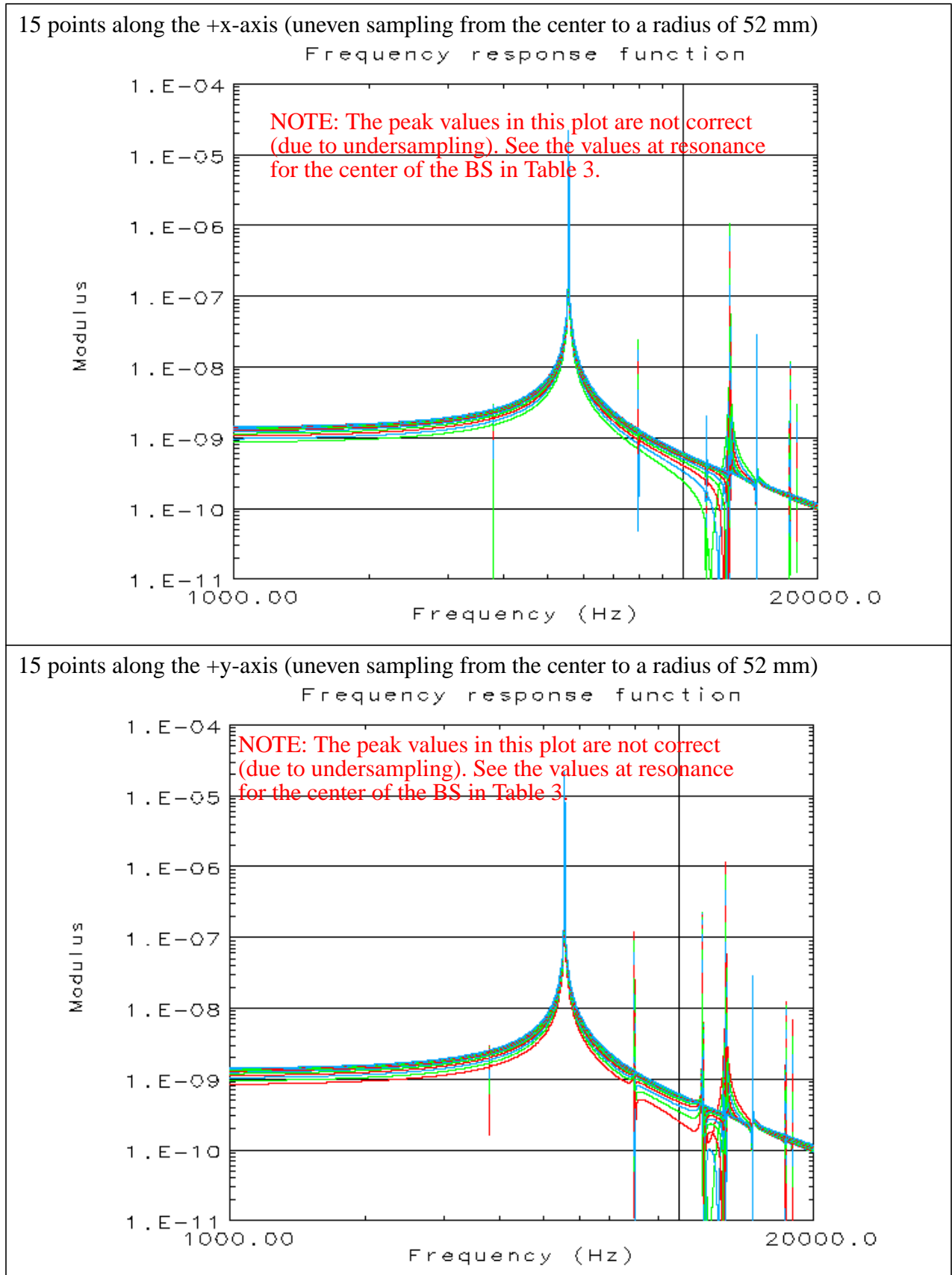
$$T_{\delta_r,k} = \frac{\Phi_{rk}(\Phi_{ke1} + \Phi_{ke2} + \Phi_{ke3} + \Phi_{ke4})}{2m_k\zeta\omega_k^2} \quad (9)$$

where:

$$\zeta = \frac{1}{2Q} = 3.8 \times 10^{-7} \quad (10)$$

Numerical values for  $\{\Phi_{ke1}, \Phi_{ke2}, \Phi_{ke3}, \Phi_{ke4}\}$ ,  $m_k$ ,  $\Phi_{kr}$  and  $T_{\delta_r,k}$  for each resonance is given in Table 3 for  $r$  = the center of the front face of the beamsplitter.

Figure (3) Magnet z-force to surface z-Displacement Transfer Function



## 5 MODE INTEGRAL OVERLAP WITH A GAUSSIAN

The derivation of the mode integral overlap with the TEM<sub>00</sub> beam has been derived previously in Ref. [1] for a normally incident beam; Here the derivation is extended to the non-normal incidence case of the beamsplitter. The cavity length change due to beamsplitter modal motion is sensed by a phase shift imparted to the TEM<sub>00</sub> mode, described by the Hermite-Gaussian function  $\Psi_{00}$ . The sensed length change is given by<sup>1</sup>:

$$\delta_{\hat{r}k} = |\hat{k}| \int_S \Psi_{00}^* \Psi_{00} \frac{(\hat{u} \cdot \hat{n})}{(\hat{k} \cdot \hat{n})} dS \quad (11)$$

where  $\hat{k}$  is the wave vector,  $\hat{n}$  is the nominal surface normal unit vector, and  $\hat{u}$  is the surface deformation vector. The product,

$$\Psi_{00}^* \Psi_{00} = I(\hat{r}) \quad (12)$$

where the Gaussian intensity distribution (normalized over the integral) is:

$$I(\hat{r}) = \left(\frac{2}{\pi w^2}\right) e^{-2\left(\frac{s}{w}\right)^2} = \left(\frac{2}{\pi w^2}\right) e^{\frac{-2[2x^2 + y^2]}{w^2}} \quad (13)$$

where the beam waist,  $w = 36.4$  mm in the recycling cavity<sup>2</sup>. In this expression,  $s$  is the radial (transverse) coordinate to the wave vector. When performing the integral over the optic surface,  $S$ , the radial coordinate must be transformed into the  $x$  and  $y$  coordinates on the face of the beamsplitter, which is nominally at a 45 degree incidence angle (hence the second equality above, where the reflection is taken about the  $y$ -axis).

The physical displacement at a position,  $r$ , on the BS surface is related to the modal displacement as follows (from Equation 5):

$$\delta_{\hat{r}k} = \Phi_{\hat{r}k} \gamma_k = \Phi_{\hat{r}k} (T_{\gamma_k} F_e) = T_{\delta_{r,k}} F_e \quad (14)$$

where the transfer function from coherent force excitation at the four magnet positions to the  $k^{\text{th}}$

---

1. The expression for the length change given in A. Gillespie and F. Raab, "Thermally excited vibrations of the mirrors of laser interferometer gravitational-wave detectors", Phys. Rev. D 52, 577(1995),

$$\text{length change} = |\hat{k}|^{-1} \int_S \Psi_{00}^* \Psi_{00} (\hat{k} \cdot \hat{u}) dS$$

is not correct in the general case of non-normal incidence. Displacement of the surface in the plane of the surface does not result in a cavity length reduction.

2. W. Kells, Core Optics Design Requirements, LIGO-T950099-04.

modal amplitude is:

$$T_{\gamma_k} = \frac{(\Phi_{ke_1} + \Phi_{ke_2} + \Phi_{ke_3} + \Phi_{ke_4})}{2m_k \zeta_k \omega_k^2} \quad (15)$$

and the transfer function from coherent force excitation at the four magnet positions to displacement at position  $r$  due to the  $k^{\text{th}}$  mode is:

$$T_{\delta_{\hat{r}k}} = \Phi_{\hat{r}k} T_{\gamma_k} \quad (16)$$

The intensity weighted integral of motion due to the  $k^{\text{th}}$  mode, over surface  $S$ , is given by:

$$\Delta_k = \int_S \delta_{\hat{r}k} I(\hat{r} - \hat{r}_o) dA = T_{\gamma_k} F_e \int_S \Phi_{\hat{r}k} I(\hat{r} - \hat{r}_o) dA \quad (17)$$

where the intensity distribution may be decentered by an alignment tolerance of  $r_o = 1$  mm:

$$\hat{r}_o = (r_o \cos \theta) \hat{i} + (r_o \sin \theta) \hat{j} \quad (18)$$

where  $i$  and  $j$  are unit vectors in the  $x$  and  $y$  coordinate directions.

The  $k^{\text{th}}$  mode integral overlap transfer function is then:

$$T_{\Delta_k} = \frac{\Delta_k}{F_e} = T_{\gamma_k} \int_S \Phi_{\hat{r}k} I(\hat{r} - \hat{r}_o) dA = T_{\gamma_k} \Gamma_k(\theta) \quad (19)$$

The maximum value of the transfer function over all values of  $\theta$  is defined as:

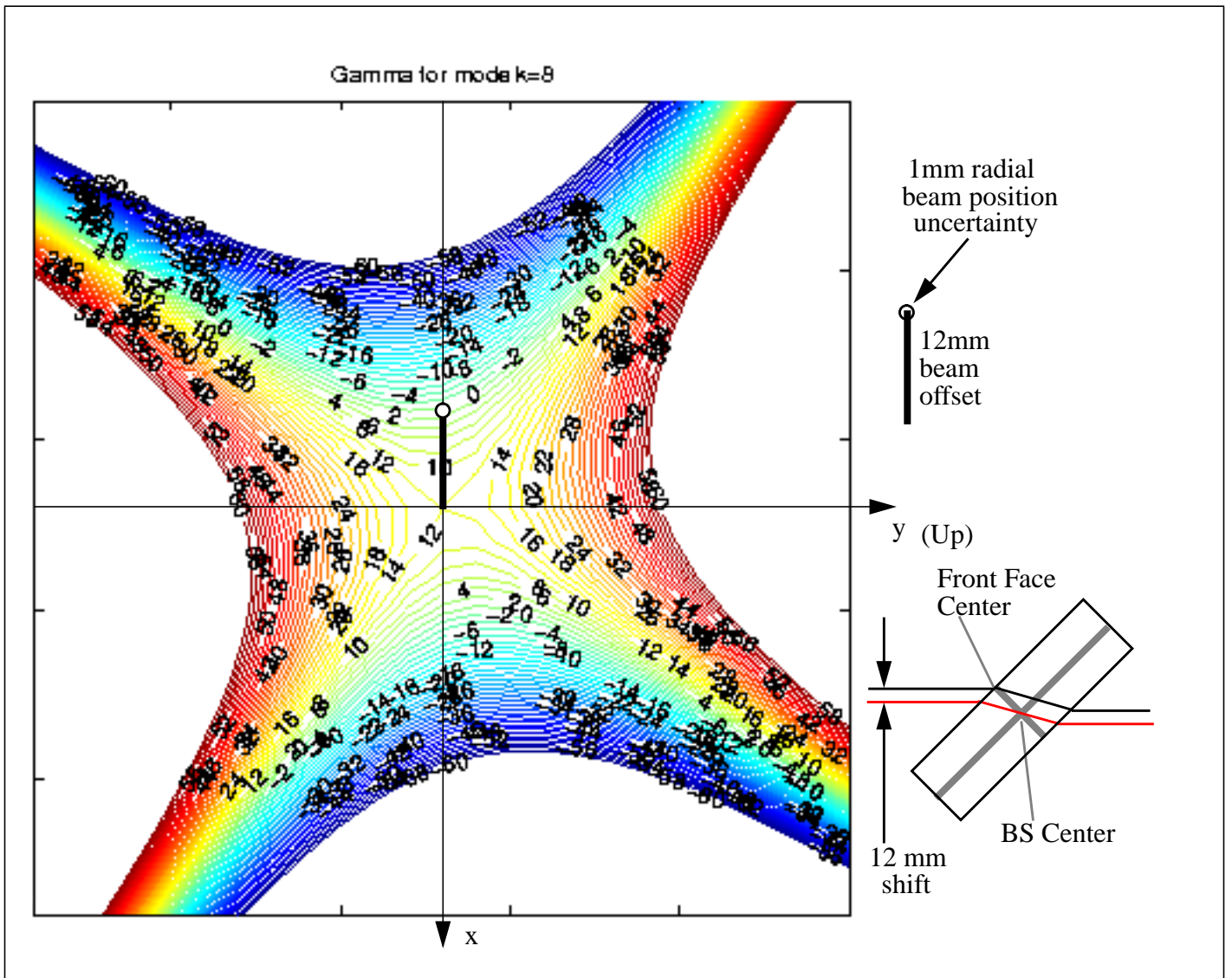
$$\max_{\theta} [T_{\Delta_k}] = T_{\gamma_k} \max_{\theta} [\Gamma_k(\theta)] \quad (20)$$

The integrals were performed in Matlab. The IDEAS finite element model (nodal positions, surface node numbers) and mode shapes were imported into Matlab. A two-dimensional spline fit to the non-uniform finite element nodal grid was used to calculate the mode shape on a finer grid within central region of  $\pm 2.4$  beam waists (i.e. the surface  $S$ ). The results (and the input and some of the intermediate values in the calculation) are given in Tables 3 and 4. The interpolated central regions,  $S$ , of the mode shapes are displayed in Table 5.

The Gaussian weighted integral transfer functions for the first 20 elastic modes are given in Table 4 for two conditions. The first condition is for a laser beam centered on the front face of the beamsplitter but with a radial alignment uncertainty of 1 mm. The second condition is an intentional horizontal ( $x$ -axis) offset (of 12 mm) such that with refraction through the beamsplitter the chief ray goes through the center of the beamsplitter, as well as a radial alignment uncertainty of 1 mm.

As indicated in Figure 4, the value of the integral is sometimes larger when the beam is centered than when it is intentionally offset by 12mm. If we take mode  $k=8$  as an example, there is approximately a factor of 5 between these two cases. In figure 4 the contour of the integral  $\Gamma_8(x, y)$  is shown as a function of the Gaussian beam offset position  $(x,y)$  where  $x$  and  $y$  range over  $\pm 50$  mm. The *possible*<sup>1</sup> horizontal offset to “compensate” for refraction through the beamsplitter (12 mm) is also indicated on the figure. For this particular mode, the value of the integral is fairly constant in the central region and 12mm offset is not large relative to this region. Furthermore, the integral decreases in the  $\pm x$ -direction relative to the center value of  $\sim 12$ , whereas the integral increases more rapidly in the  $\pm y$ -direction. The difference in gradient in these two directions is probably due to the wedge (which is aligned in the  $y$ -direction, thick side “up”). The slight rotation ( $\sim 5$  degrees) of modes 7 and 8 from the symmetry plane ( $y$ -axis) is strange and may be a numerical artifact.

Figure (4) Contour of the Integral  $\Gamma_8(x, y)$  for the Gaussian Beam Center at  $(x,y)$  where the beam offset range is  $\pm 50$ mm for both  $x$  and  $y$

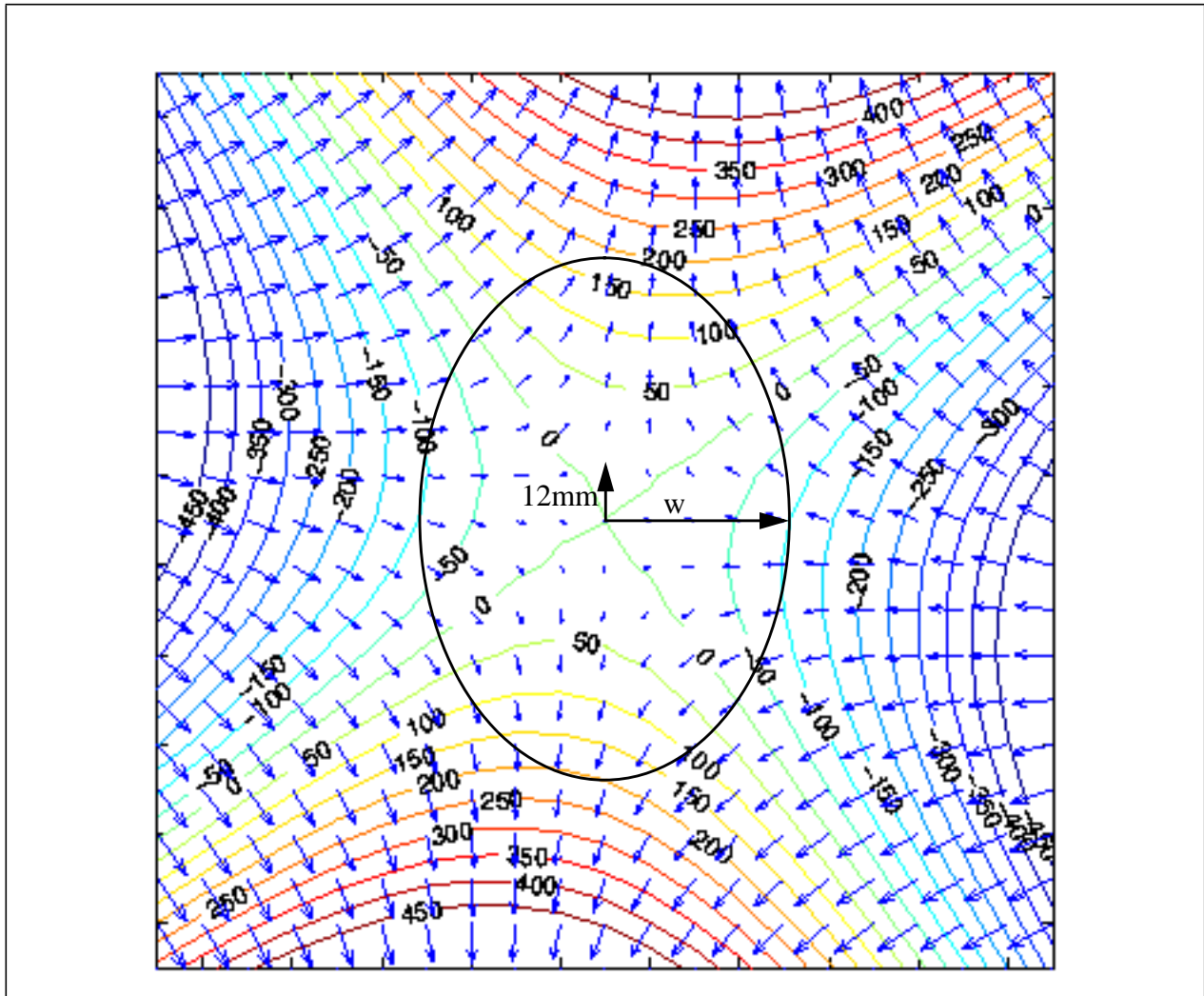


1. Nominally the laser is centered on the front, high-reflectance (HR) surface  $\pm 1$ mm



The reason that the integral is positive and non-zero when the beam is centered, can be seen in Figure 5, where the  $z$ -displacement (displacement in the direction of the cylindrical axis) is contour plotted. An ellipse with a minor axis radius equal to the beam waist, and centered on the beamsplitter, is overlaid on the contour plot. The extent of the ellipse left/right (along the  $\pm y$ -axis) is almost equal  $\{-105, -105\}$ , whereas the extent of the ellipse up/down (along the  $\pm x$ -axis) is greater and not equal  $\{+205, +190\}$ . Consequently, a small (because the Gaussian is rapidly decreasing with radius) positive integral results.

Figure (5) The  $z$ -displacement of the surface (interpolated) for the  $k=8$  mode (The circle is centered on the BS and has a radius equal to the beam waist,  $w$ .)



The transfer function at the BS first symmetric mode (5578 Hz) is about 10 times greater than for the ITM at its first symmetric mode (9205 Hz).

**Table 3. Front Surface Center Transfer Function (modal damping,  $\zeta = 3.8 \times 10^{-7}$ )**

$k$	Frequency (Hz)	Modal Mass ( $10^6$ gm)	Mode Shape Amplitude at Magnet Positions				Modal Transfer Function $T_{\gamma_k}$	Mode Shape Amplitude at the Center $\Phi_{kr}$	Center Displacement $T_{\delta,k}$ (m/N)
			$\Phi_{ke_1}$	$\Phi_{ke_2}$	$\Phi_{ke_3}$	$\Phi_{ke_4}$			
7	3784.9	8.65e+05	-770.53	769.90	817.05	-816.13	7.72e-10	-332.51	-2.57e-07
8	3784.9	8.51e+05	260.66	-262.49	-276.00	278.65	2.23e-09	243.77	5.44e-07
9	5578.2	1.25e+06	-527.56	-527.56	-562.12	-562.12	-1.87e-06	151.04	-2.82e-04
10	7974.7	7.35e+05	246.17	729.02	-778.86	-286.95	-6.46e-08	-44.07	2.85e-06
11	7974.8	7.56e+05	-748.33	275.57	-263.23	779.93	3.05e-08	-313.70	-9.56e-06
12	11259.1	2.17e+06	10.34	18.61	-15.25	-15.16	-1.77e-10	-21.41	3.78e-09
13	11259.1	3.26e+06	-27.35	19.70	3.75	4.28	3.09e-11	35.19	1.09e-09
14	11332.3	1.08e+06	371.77	371.60	-387.98	-388.18	-7.88e-09	-492.48	3.88e-06
15	11334.2	1.13e+06	371.40	-371.59	405.78	-405.58	2.07e-12	-363.88	-7.52e-10
16	12674.4	1.16e+06	-29.80	-29.81	23.89	23.87	-2.12e-09	17.73	-3.75e-08
17	12677.4	1.11e+06	-21.77	21.69	-31.35	31.30	-2.24e-11	14.51	-3.25e-10
18	12760.0	7.02e+05	457.64	418.74	481.24	439.72	5.24e-07	235.12	1.23e-04
19	12760.1	6.51e+05	-611.23	-636.55	-642.13	-669.20	-8.05e-07	-76.96	6.19e-05
20	14628.5	3.20e+06	-35.04	-35.04	-46.48	-46.48	-7.93e-09	59.76	-4.74e-07
21	17283.2	1.46e+06	3.93	-31.62	21.75	21.08	1.16e-09	-33.87	-3.92e-08

**Table 3. Front Surface Center Transfer Function (modal damping,  $\zeta = 3.8 \times 10^{-7}$ )**

$k$	Frequency (Hz)	Modal Mass ( $10^6$ gm)	Mode Shape Amplitude at Magnet Positions				Modal Transfer Function $T_{\gamma_k}$	Mode Shape Amplitude at the Center $\Phi_{kr}$	Center Displacement $T_{\delta_{\gamma k}}$ (m/N)
			$\Phi_{ke_1}$	$\Phi_{ke_2}$	$\Phi_{ke_3}$	$\Phi_{ke_4}$			
22	17283.3	1.56e+06	-41.21	25.42	11.60	12.82	6.17e-10	39.63	2.45e-08
23	17388.4	1.15e+06	385.10	-394.31	-412.13	421.19	-1.36e-11	-580.75	7.90e-09
24	17388.4	1.15e+06	-212.33	194.82	226.25	-209.07	-3.09e-11	606.65	-1.87e-08
25	17958.0	5.75e+05	728.49	3.59	55.42	-764.36	4.16e-09	120.00	4.99e-07
26	17958.3	5.76e+05	52.53	730.77	-762.80	4.32	4.45e-09	135.46	6.03e-07

**Table 4. Gaussian Weighted Integral Transfer Function**

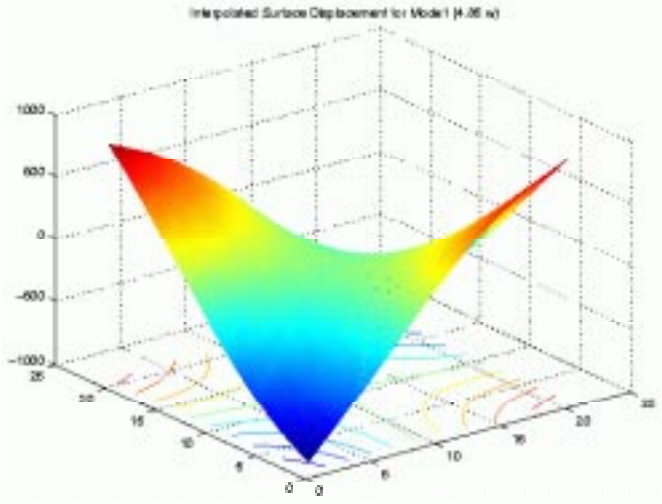
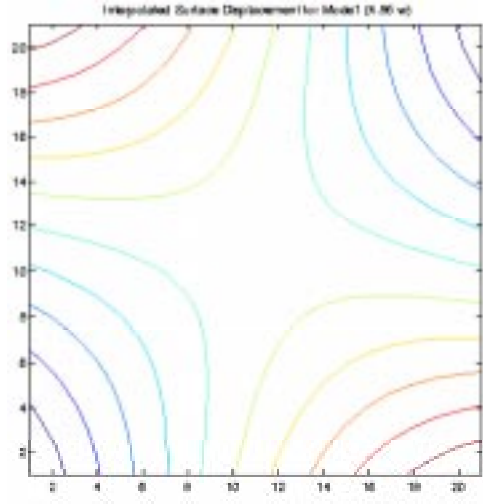
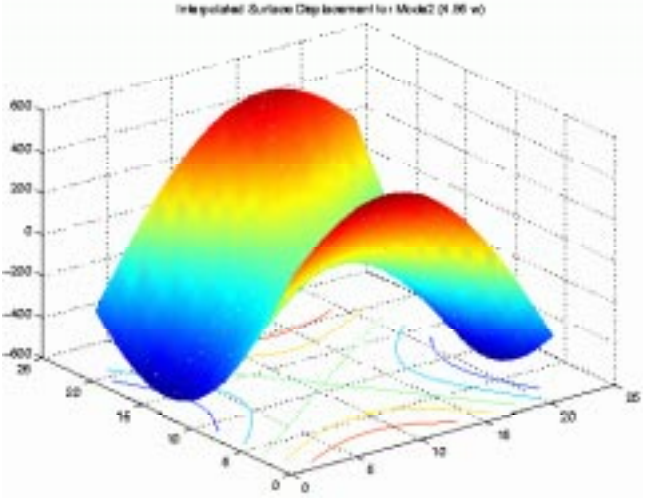
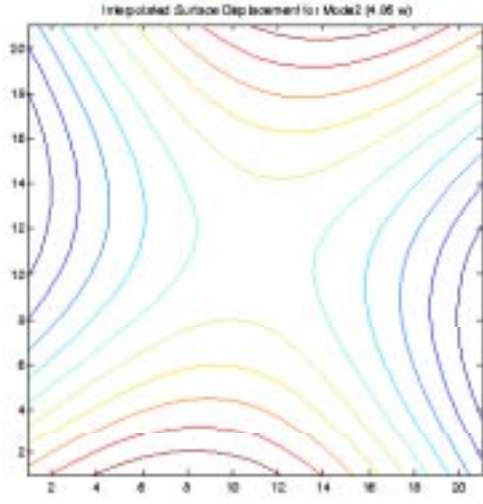
$k$	Frequency (Hz)	Value of the Integral with no Gaussian Intensity Distribution offset $\Gamma_k(r_o \rightarrow 0)$	Centered $\oplus \varnothing 1 \text{ mm}$		Refractive Offset (12 mm offset in $x$ $\oplus \varnothing 1 \text{ mm}$ )	
			Maximum Value of the Integral vs. $\theta$ $\max_{\theta}[ \Gamma_k(\theta) ]$	Gaussian Weighted Integral Transfer Function $\max_{\theta}[T_{\Delta_k}]$ (m/N)	Maximum Value of the Integral vs. $\theta$ $\max_{\theta}[ \Gamma_k(\theta) ]$	Gaussian Weighted Integral Transfer Function $\max_{\theta}[T_{\Delta_k}]$ (m/N)
7	3784.9	4.131	4.336	3.35e-09	3.920	3.03e-09
8	3784.9	12.007	12.224	2.73e-08	2.575	5.75e-09
9	5578.2	893.064	893.143	-1.67e-03	873.596	-1.63e-03
10	7974.7	0.052	0.449	-2.90e-08	1.471	-9.51e-08
11	7974.8	-0.021	0.425	1.29e-08	3.140	9.56e-08
12	11259.1	-0.174	1.303	-2.30e-10	3.948	-6.97e-10
13	11259.1	0.046	1.467	4.52e-11	17.916	5.53e-10
14	11332.3	-1.554	26.134	-2.06e-07	25.681	-2.02e-07
15	11334.2	-0.006	26.652	5.51e-11	336.297	6.95e-10
16	12674.4	3.312	3.749	-7.94e-09	3.564	-7.55e-09
17	12677.4	0.001	0.431	-9.63e-12	5.571	-1.25e-10
18	12760.0	-0.384	0.394	2.06e-07	0.362	1.90e-07
19	12760.1	0.558	0.566	-4.56e-07	0.403	-3.24e-07
20	14628.5	114.422	114.492	-9.08e-07	113.565	-9.01e-07
21	17283.2	-2.963	2.999	3.47e-09	0.750	8.69e-10
22	17283.3	-1.691	1.728	1.07e-09	0.604	3.73e-10

**Table 4. Gaussian Weighted Integral Transfer Function**

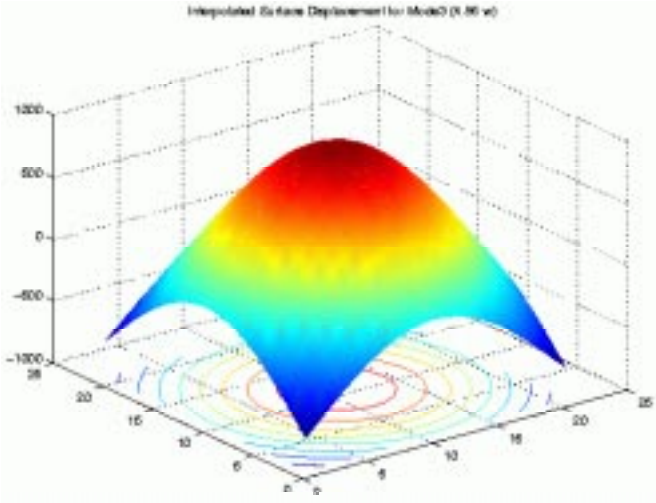
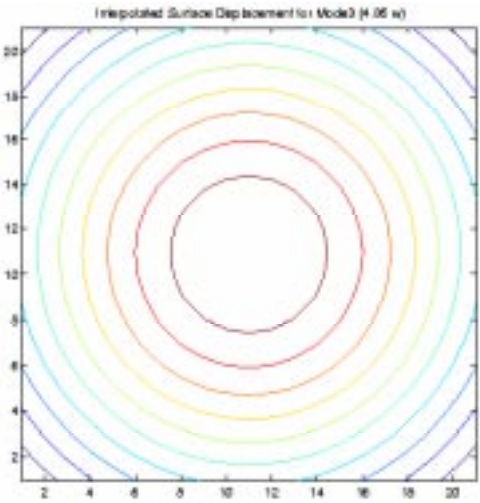
$k$	Frequency (Hz)	Value of the Integral with no Gaussian Intensity Distribution offset $\Gamma_k(r_o \rightarrow 0)$	Centered $\oplus \varnothing 1 \text{ mm}$		Refractive Offset (12 mm offset in $x$ $\oplus \varnothing 1 \text{ mm}$ )	
			Maximum Value of the Integral vs. $\theta$ $\max_{\theta}[ \Gamma_k(\theta) ]$	Gaussian Weighted Integral Transfer Function $\max_{\theta}[T_{\Delta_k}]$ (m/N)	Maximum Value of the Integral vs. $\theta$ $\max_{\theta}[ \Gamma_k(\theta) ]$	Gaussian Weighted Integral Transfer Function $\max_{\theta}[T_{\Delta_k}]$ (m/N)
23	17388.4	31.026	31.568	-4.30e-10	10.612	-1.44e-10
24	17388.4	59.528	60.067	-1.85e-09	14.029	-4.33e-10
25	17958.0	0.006	0.039	1.64e-10	0.126	5.23e-10
26	17958.3	0.004	0.037	1.65e-10	0.153	6.81e-10

The table below shows the interpolated surface displacements for each of the first 20 elastic modes of the beamsplitter.

**Table 5. Interpolated Mode Shapes for Z-displacement of the Front Surface Central Region ( $\pm 2.43 w$ )**

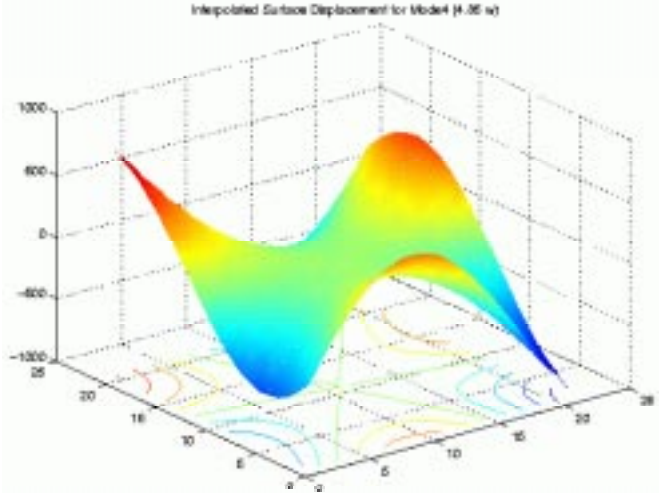
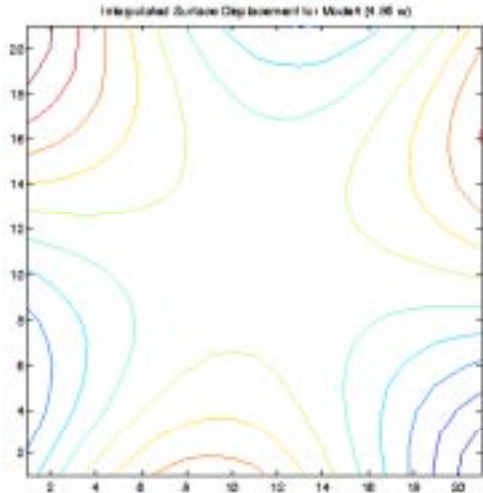
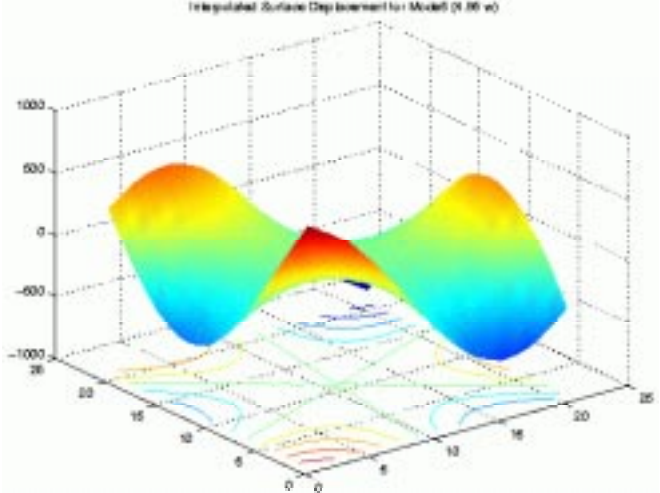
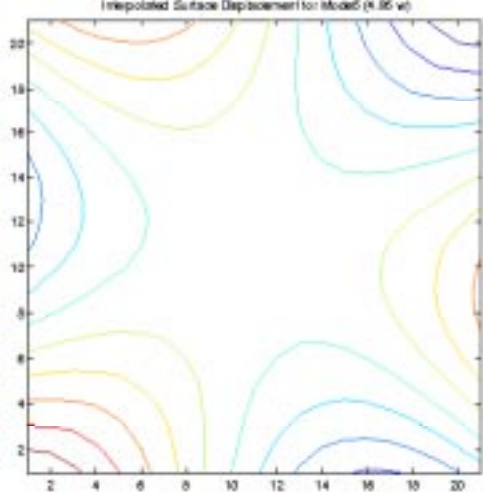
$k$	Frequency (Hz)	Surface Plot	Contour Plot
7	3785	 <p>Interpolated Surface Displacement for Mode1 (3785 Hz)</p>	 <p>Interpolated Surface Displacement for Mode1 (3785 Hz)</p>
8	3785	 <p>Interpolated Surface Displacement for Mode2 (3785 Hz)</p>	 <p>Interpolated Surface Displacement for Mode2 (3785 Hz)</p>

**Table 5. Interpolated Mode Shapes for Z-displacement of the Front Surface Central Region ( $\pm 2.43 w$ )**

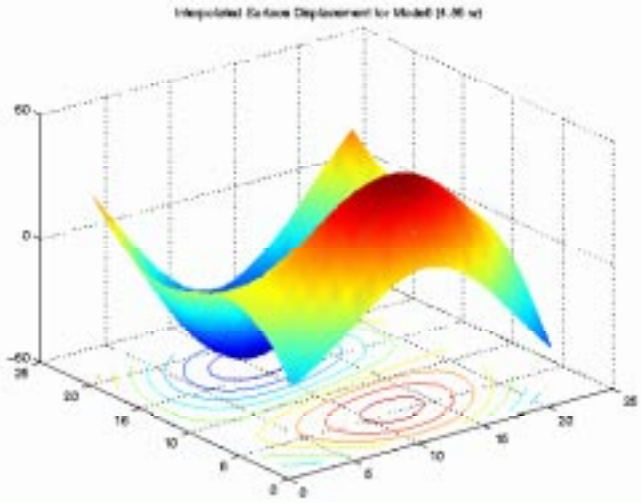
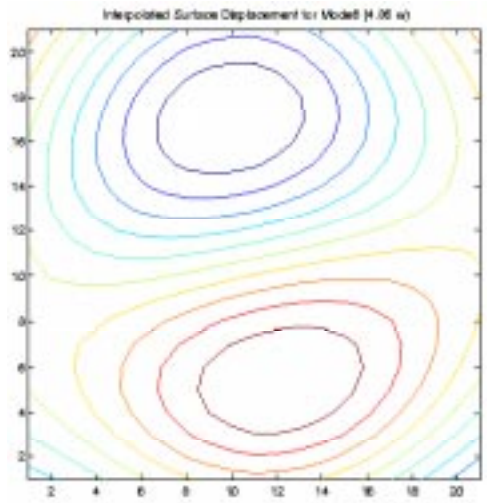
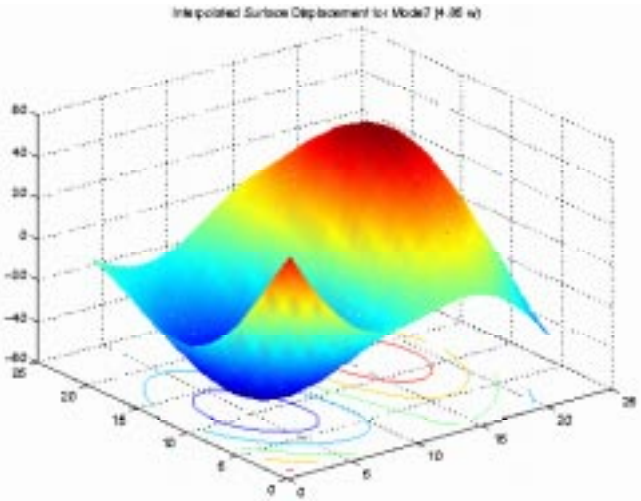
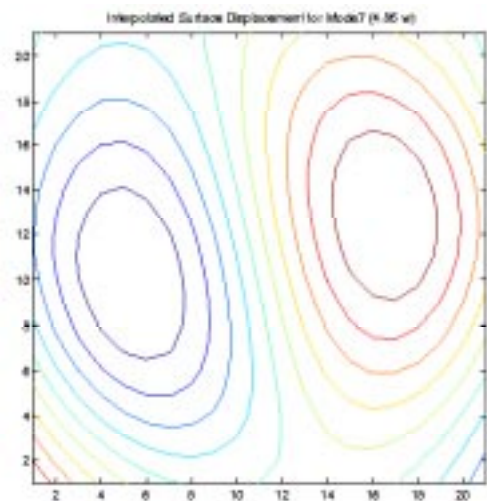
$k$	Frequency (Hz)	Surface Plot	Contour Plot
9	5578	 <p>Interpolated Surface Displacement for Mode9 (4.06 w)</p>	 <p>Interpolated Surface Displacement for Mode9 (4.06 w)</p>



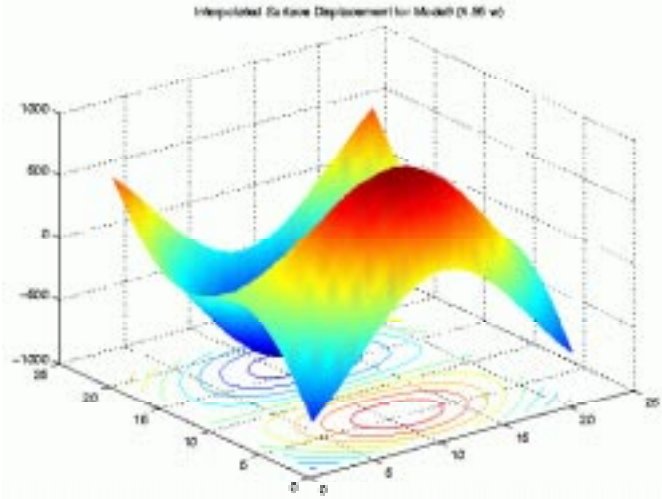
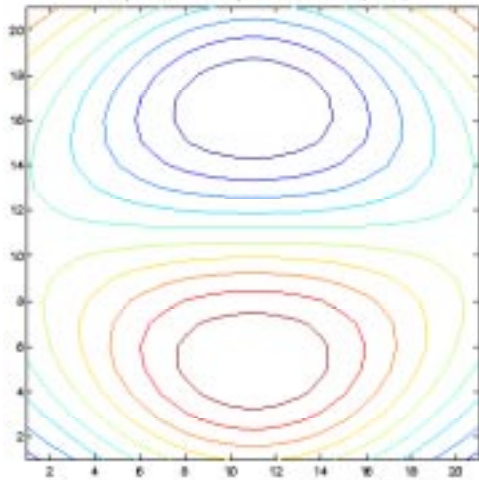
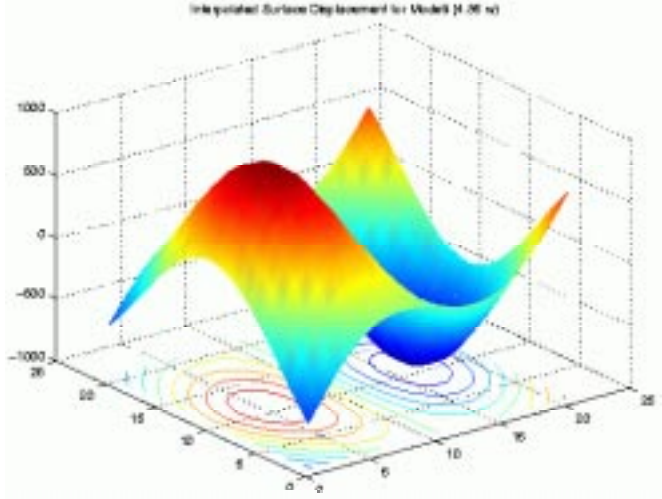
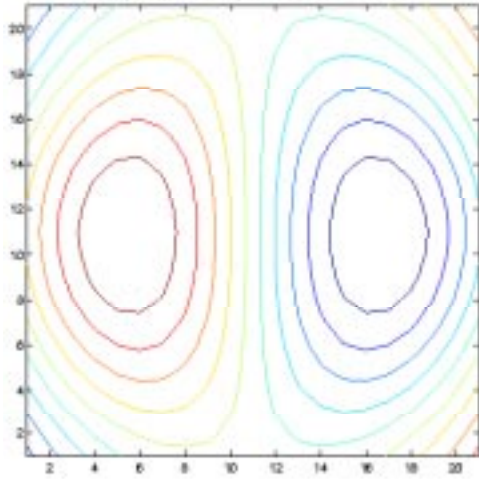
**Table 5. Interpolated Mode Shapes for Z-displacement of the Front Surface Central Region ( $\pm 2.43 w$ )**

$k$	Frequency (Hz)	Surface Plot	Contour Plot
10	7975	 <p>Interpolated Surface Displacement for Model4 (4.86 w)</p>	 <p>Interpolated Surface Displacement for Model4 (4.86 w)</p>
11	7975	 <p>Interpolated Surface Displacement for Model4 (4.86 w)</p>	 <p>Interpolated Surface Displacement for Model4 (4.86 w)</p>

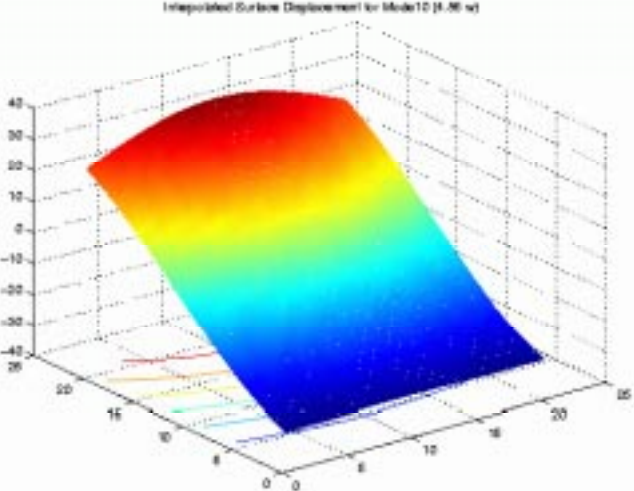
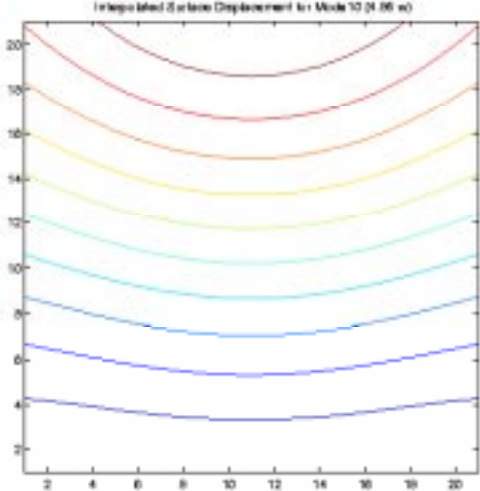
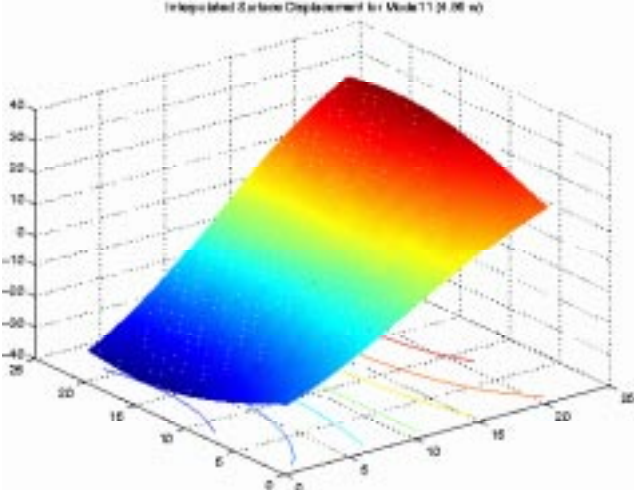
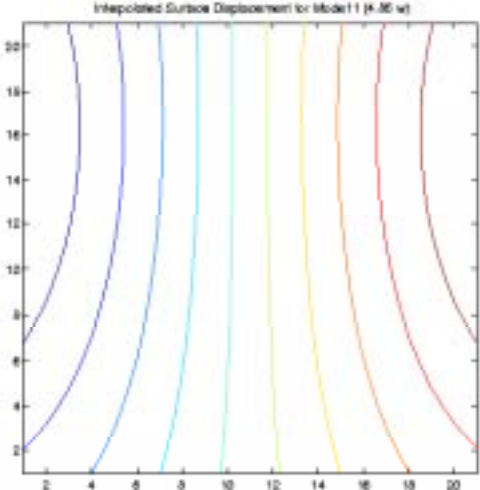
**Table 5. Interpolated Mode Shapes for Z-displacement of the Front Surface Central Region ( $\pm 2.43 w$ )**

$k$	Frequency (Hz)	Surface Plot	Contour Plot
12	11259	 <p>Interpolated Surface Displacement for Mode6 (11.26 w)</p>	 <p>Interpolated Surface Displacement for Mode6 (11.26 w)</p>
13	11259	 <p>Interpolated Surface Displacement for Mode7 (11.26 w)</p>	 <p>Interpolated Surface Displacement for Mode7 (11.26 w)</p>

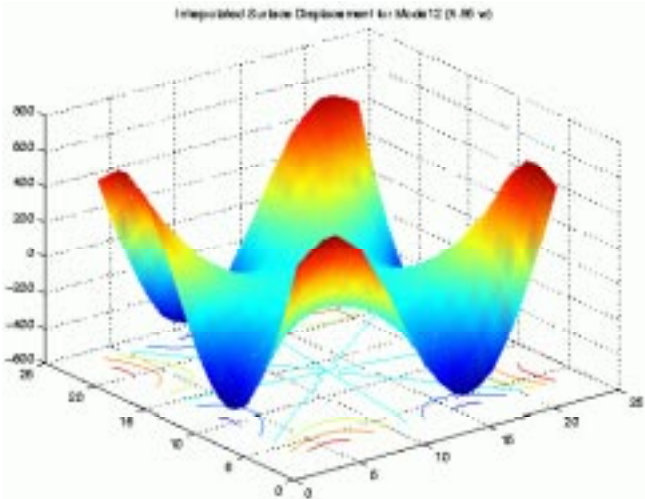
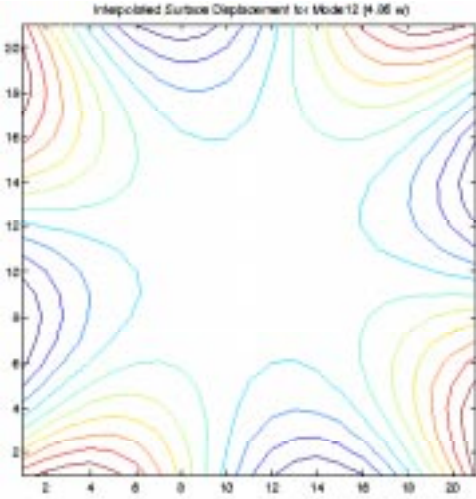
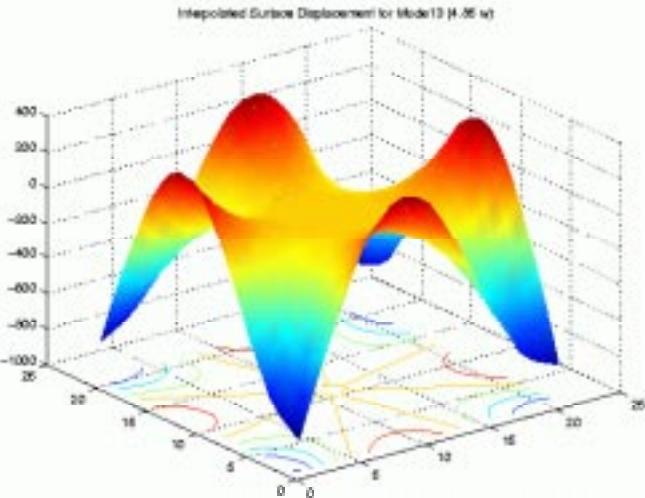
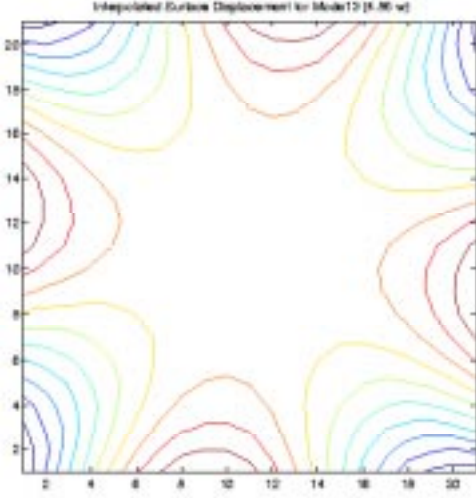
**Table 5. Interpolated Mode Shapes for Z-displacement of the Front Surface Central Region ( $\pm 2.43 w$ )**

$k$	Frequency (Hz)	Surface Plot	Contour Plot
14	11332		
15	11334		

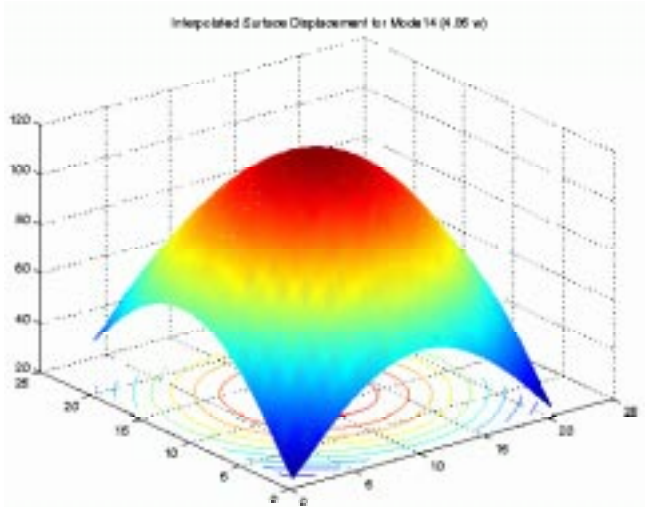
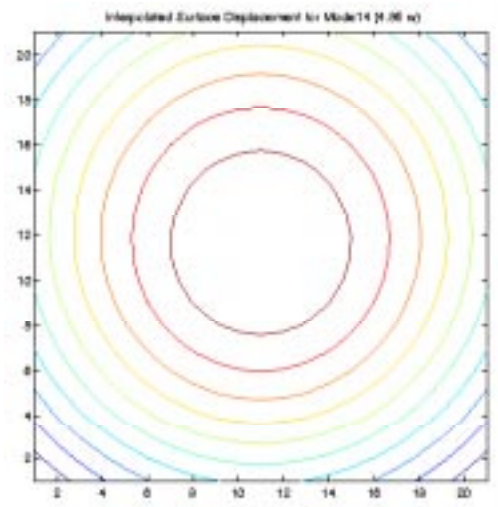
**Table 5. Interpolated Mode Shapes for Z-displacement of the Front Surface Central Region ( $\pm 2.43 w$ )**

$k$	Frequency (Hz)	Surface Plot	Contour Plot
16	12674		
17	12677		

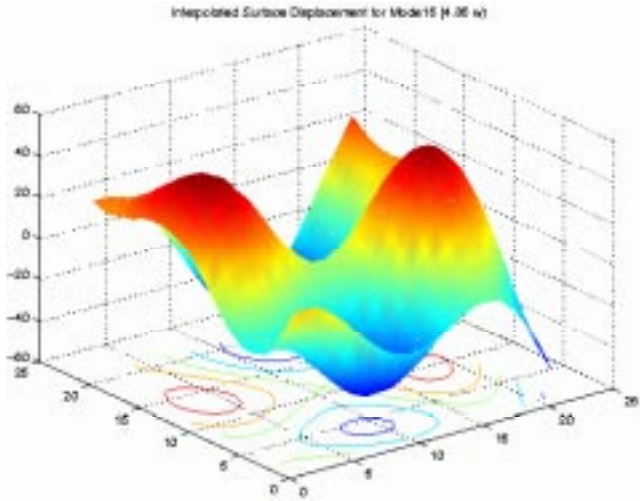
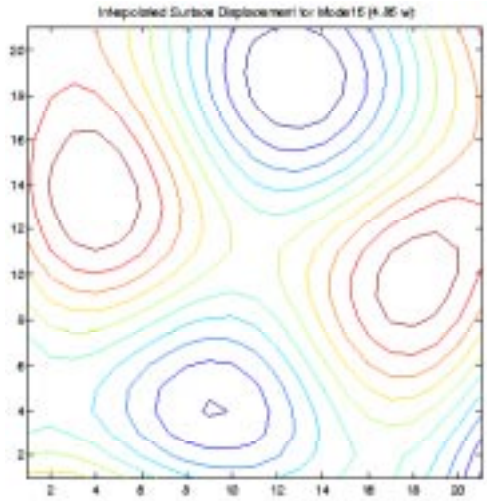
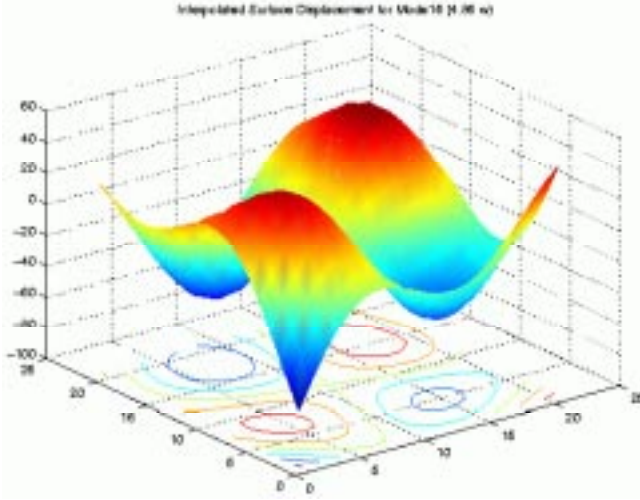
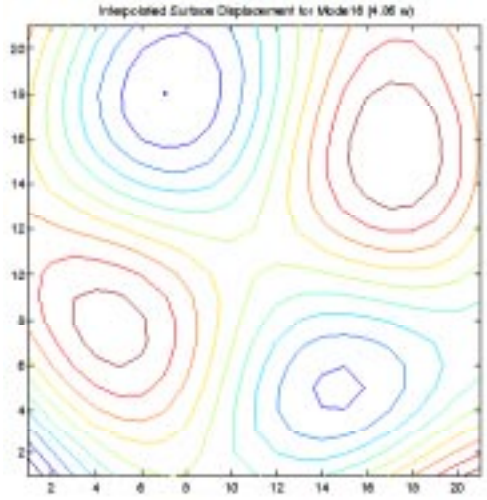
**Table 5. Interpolated Mode Shapes for Z-displacement of the Front Surface Central Region ( $\pm 2.43 w$ )**

$k$	Frequency (Hz)	Surface Plot	Contour Plot
18	12760		
19	12760		

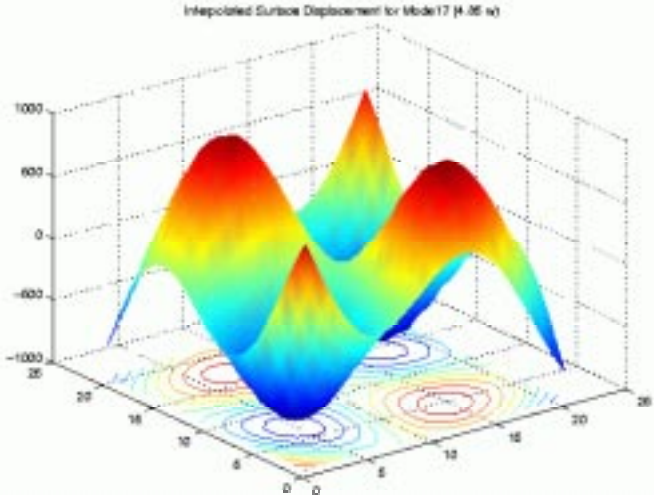
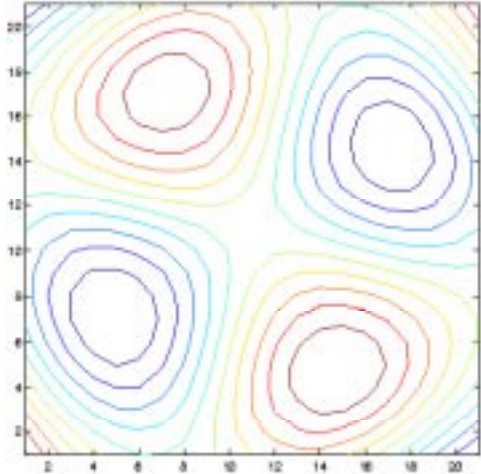
**Table 5. Interpolated Mode Shapes for Z-displacement of the Front Surface Central Region ( $\pm 2.43 w$ )**

$k$	Frequency (Hz)	Surface Plot	Contour Plot
20	14628	 <p>Interpolated Surface Displacement for Mode 14 (14.66 w)</p>	 <p>Interpolated Surface Displacement for Mode 14 (14.66 w)</p>

**Table 5. Interpolated Mode Shapes for Z-displacement of the Front Surface Central Region ( $\pm 2.43 w$ )**

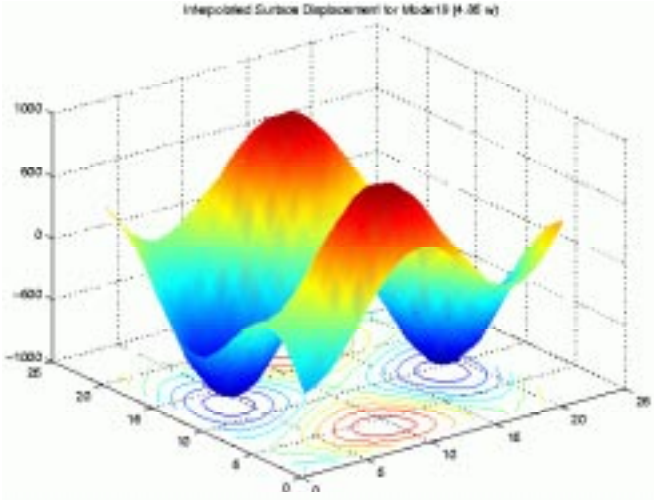
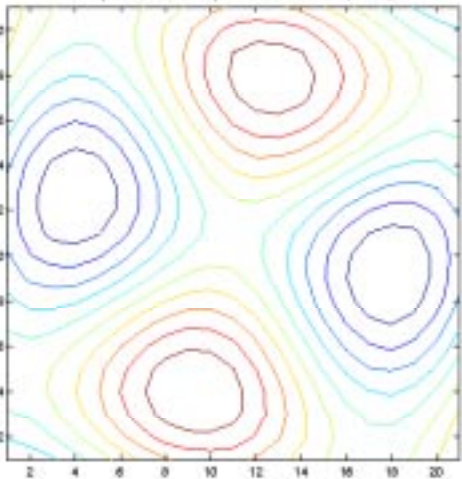
$k$	Frequency (Hz)	Surface Plot	Contour Plot
21	17283		
22	17283		

**Table 5. Interpolated Mode Shapes for Z-displacement of the Front Surface Central Region ( $\pm 2.43 w$ )**

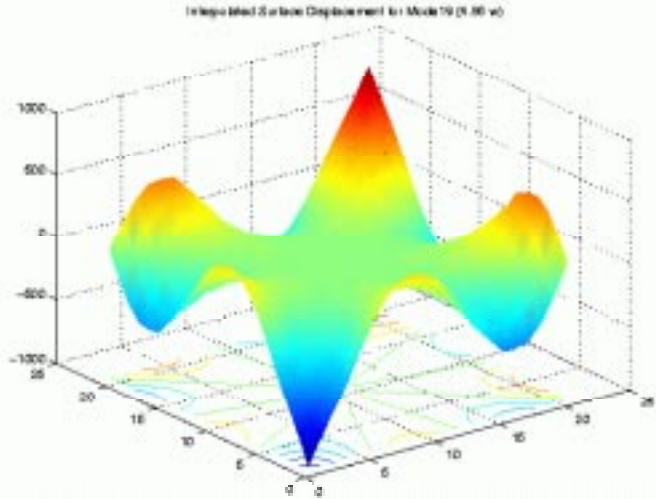
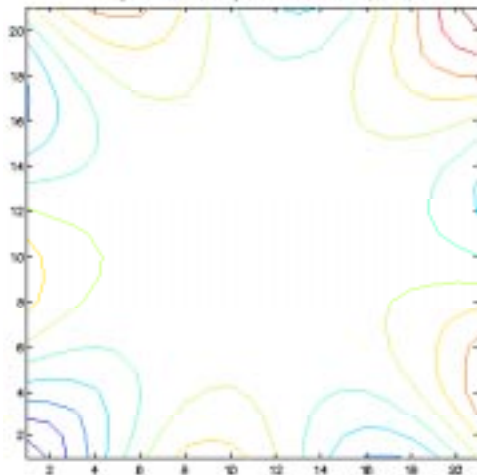
$k$	Frequency (Hz)	Surface Plot	Contour Plot
23	17388	 <p>Interpolated Surface Displacement for Mode 17 (17.388 Hz)</p>	 <p>Interpolated Surface Displacement for Mode 17 (17.388 Hz)</p>



**Table 5. Interpolated Mode Shapes for Z-displacement of the Front Surface Central Region ( $\pm 2.43 w$ )**

$k$	Frequency (Hz)	Surface Plot	Contour Plot
24	17388		

**Table 5. Interpolated Mode Shapes for Z-displacement of the Front Surface Central Region ( $\pm 2.43 w$ )**

$k$	Frequency (Hz)	Surface Plot	Contour Plot
25	17958		
26	17958	